



Contents lists available at ScienceDirect

Journal of Sound and Vibration

journal homepage: www.elsevier.com/locate/jsv

Investigation on the dominant mechanism of chatter in high-load robot milling process based on theoretical and experimental analysis

Yuchao Du^a, Zhiqiang Liang^{a,b,*}, Zirui Gao^a, Sichen Chen^a, Yi Yue^c, Jiabo Zhang^c, Hanliang Liu^c, Haoran Zheng^a, Baolong Liu^a, Tianyang Qiu^a, Zhibing Liu^a

^a School of Mechanical Engineering, Beijing Institute of Technology, Beijing 100081, PR China

^b Beijing Institute of Technology, Zhengzhou Academy of Intelligent Technology, Zhengzhou 450000, PR China

^c Beijing Spacecrafts, Beijing 100094, PR China

ARTICLE INFO

Keywords:

High-load robotic milling
Milling chatter
Chatter dominant mechanism
Mode coupling chatter
Regenerative chatter

ABSTRACT

Chatter has always been a key problem restricting the improvement of robotic milling quality and efficiency. To avoid chatter, it is necessary to determine what is the dominant chatter mechanism (mode coupling or regenerative) of the robot milling system. Therefore, this paper focus on the dominant chatter mechanism in high-load (600kg) robot milling. The modal test results show that the dynamic flexibility of spindle-tool structure mode in high-load robot is significantly higher than that of the body structure mode, which is significantly different from the low-load robot in other studies. The mode coupling chatter stability prediction models are established based on eigenvalue method and zeroth order approximation, and the predicted stability boundaries are compared with the experimental results. The results show that only high-frequency chatter exists in the high speed region (1000–8000rpm), and no low frequency chatter occurs. The low-frequency chatter around the robot body mode is found in the low-speed region (400–1000rpm), but the mode coupling chatter theory could not explain the chatter varies periodically with the spindle speed. However, the stability boundary predicted by the regenerative chatter theory also changes periodically with the spindle speed. This indicates that the milling chatter dominant mechanism of high load robot is regenerative chatter. This study analyzes the milling chatter dominant mechanism of high-load robot through theoretical and experimental verification, which can provide theoretical support for high-load robot milling chatter control.

1. Introduction

The development of high-end equipment is increasingly developing in the direction of large-scale and complicated, with the rapid development of industry [1–3]. Industrial robots are desired to be widely used in machining large and complex structural parts due to their advantages of high flexibility, strong flexibility, and good spatial accessibility [4–6]. However, the structural characteristics of the robot make it easy to generate self-excited chatter when it is subjected to periodic external excitation, which will greatly reduce the

* Corresponding author.

E-mail address: liangzhiqiang@bit.edu.cn (Z. Liang).

<https://doi.org/10.1016/j.jsv.2024.118886>

Received 18 June 2024; Received in revised form 22 September 2024; Accepted 28 November 2024

Available online 29 November 2024

0022-460X/© 2024 Elsevier Ltd. All rights are reserved, including those for text and data mining, AI training, and similar technologies.

machining accuracy, efficiency, and surface quality, and even cause rapid tool wear and machine damage, this is one of the main problems restricting the application of robots [7–10]. Therefore, effectively controlling the milling chatter of the robot to keep it in a stable processing state is of great significance to improve the milling quality and efficiency of the robot.

The existing studies show that there are two main self-excited vibration mechanisms in robot milling: regenerative chatter and mode coupling chatter [11]. Regenerative chatter is the self-excited vibration caused by the difference of cutting thickness caused by the phase difference between the vibration marks formed by the previous cutting teeth and the vibration displacement of the current cutting teeth [12]. Due to the low stiffness characteristic of the robot milling system, vibration marks are left on the machined surface by the action of aperiodic milling force. When the tool teeth repeatedly cut on the vibrating surface, resulting in a modulation of chip thickness, which excites the regenerative chatter. In the robotic milling process, regenerative chatter is considered to be generated by the excitation of spindle-tool high frequency mode, which is manifested as a kind of high frequency chatter [13].

The mode coupling effect may occur if the natural modes are closely matched in principal directions. Without any regeneration, the structure vibrates simultaneously in the different directions at the same frequency and a phase shift [14]. Therefore, mode coupling chatter is considered to be generated when the tool is cutting on a new surface, which generally occurs in threading [15]. Mode coupling chatter in robotic milling was first reported in the research of Pan [16]. In Pan et al.'s study, low-frequency chatter signals surrounding low-frequency modes of robot body structure were found during robot milling. He believed that the mode coupling chatter of robot milling occurs because the robot structure stiffness is not significantly higher than the process stiffness.

In terms of regenerative chatter control in robot milling, a common method is to build a robot milling stability prediction model based on the regenerative chatter theory to predict the chatter stability boundary, so as to guide the selection of process parameters to avoid the occurrence of regenerative chatter. M.Cordes et al. [13] established a robot milling dynamic model considering multi-mode coupling and structural mode coupling effects, and realized the prediction of chatter stability boundary. It is worth noting that “mode coupling” should not be confused with “mode coupling chatter”. Mode coupling refers to the phenomenon of coupling of modes of vibration with closely spaced natural frequencies when the structure is under free vibration. Whereas, mode coupling chatter is a specific type of self-excited vibration. Wang et al. [17] found that the robot milling system has low-frequency cross modes. In the milling dynamics modeling, not only the x and y direction mode parameters were considered, but also the xy direction and yx direction low-frequency mode parameters were further introduced, and the milling dynamics model considering the mode coupling effect of the low-frequency structure was constructed to achieve the prediction of chatter stability boundary. Xin et al. [18,19] studied the influence of robot structural modes on chatter stability, established a milling dynamics model considering robot low-frequency vibration, and predicted the chatter stability boundary of robot milling more accurately. Y.Mohammadi et al. [20,21] established a nonlinear regenerative dynamic force model considering axial vibration, and the experimental results show that the chatter stability prediction is more accurate when the axial vibration is considered. Based on the regenerative chatter theory, Du et al. [22] constructed a robot milling dynamic model considering force-induced deformation, which further improved the prediction accuracy of chatter stability. In addition, Celikag et al. [23] and Mousavi et al. [24,25] studied the optimization of robot configuration by controlling robot functional redundancy to improve robotic milling regenerative chatter stability. Chen et al. [26] designed a vortex damper on the robot spindle to suppress tool tip vibration during machining, and built a robot milling dynamic model considering the vortex damping effect to realize the suppression of high-frequency tool tip chatter. Sun et al. [27] used rotary ultrasonic vibration assisted milling to suppress regenerative chatter in robot milling.

In terms of mode coupling chatter control for robot milling, based on the theory of mode coupling chatter, He et al. [28] established the stability criterion of mode coupling chatter, and optimized the milling path to realize the suppression of mode coupling chatter. Gienke et al. [29] proposed an extended mode coupling chatter prediction theory considering robot kinematics, and realized the suppression of mode coupling chatter by controlling the magnitude and direction of cutting force. Pan et al. [30] established the stability criterion of mode coupling chatter to guide the selection of machining configuration and parameters to achieve non-flutter machining. Cen et al. [31] also predicted the occurrence conditions of chatter based on the mode coupling chatter theory, and proposed a stiffness optimization method based on Conservative Congruence Transformation. This method does not need to change the machining path of the robot to realize the suppression of mode coupling chatter. Cen et al. [32] proposed a detection method for mode coupling chatter in robot milling based on instantaneous force-induced dynamic strain signals, and optimized the milling path according to the detection results to achieve mode coupling chatter suppression. Based on the low frequency characteristics of mode coupling chatter, Yuan et al. [33] designed a semi-active magnetorheological elastomers absorber to suppress mode coupling chatter during robot milling process.

The above research indicate that both parameter selection based on chatter prediction results and suppression of chatter components at specific frequencies depend on the identification of the dominant chatter mechanism. However, there are few research on chatter control of high-load robot (600 kg) milling (The existing research often use robots with a load of about 200kg). The dynamic characteristics of high-load robots are quite different from those of low-load robots (For example, there will be significant differences in the stiffness of the body structure), which may affect the milling chatter behavior. Therefore, this paper focus on the investigation of the dominant chatter mechanism in high-load robot milling. The difference between the dynamic characteristics of high load robot milling system and low load robot is analyzed. Based on eigenvalue method (EM) and zeroth order approximation (ZOA), the stability prediction models of mode coupling chatter are established, and the predicted stability boundaries are compared with the experimental results. The dominant mechanism of milling chatter is revealed based on a comparative analysis of theory and experiment, which can provide theoretical support for high-load robot milling chatter control.

2. Dynamic characteristics analysis of the high-load robotic milling system

The dynamic characteristic of milling system is an indispensable physical quantity for chatter stability analysis [34]. In order to explore the dominant mechanism of chatter in high-load robotic milling process, dynamic characteristic tests are carried out in this section. The KUKA KR600 industrial robot is selected. The robot has a rated load of 600kg and a maximum load capacity of 729kg, which is a typical high-load robot. The end of the robot is equipped with high-speed electric spindle (HCS150lg-20K), the end of the spindle is equipped with 10mm three-tooth carbide end mill, and the tool overhang is set to 60mm. The posture of the robot is selected to be consistent with the machining process, which are $\theta_1 = -77.78^\circ$, $\theta_2 = -61.23^\circ$, $\theta_3 = 100.68^\circ$, $\theta_4 = 13.87^\circ$, $\theta_5 = -40.70^\circ$ and $\theta_6 = -220.71^\circ$. The force hammer installed with YD-5T quartz sensor is used to hammer the tool tip to generate the excitation signal, and the output signal is collected by the eddy current sensor. The frequency response function (FRF) in x direction and y direction are tested, respectively. Where, the x direction and y direction are the defined direction of the workpiece coordinate system. The dynamic characteristic testing process of the robot milling system is shown in Fig. 1.

The FRFs at the tool tip of the robot milling system obtained by the tests are shown in Fig. 2. It can be seen that the robot milling system has two dominant modes, respectively in the low frequency region and the high frequency region. Its low-frequency dominant mode is concentrated in 15–20Hz, as shown in Fig. 2(a) and the high-frequency dominant mode is concentrated above 2000Hz, as shown in Fig. 2(b). The low frequency mode is related to the robot body structure, while the high frequency mode is related to the spindle-tool structure [35]. Existing studies on mode coupling chatter in robot milling show that mode coupling chatter is low-frequency chatter, and its chatter frequency is around the low-frequency dominant mode of the robot [31].

The difference between the dynamic characteristics of the high-load robot and those of other studies is further compared, as shown in Fig. 3. It can be seen that the dynamic characteristics of the high-load robot used in this study are different from other studies. The dynamic flexibility of the high-frequency mode is significantly higher than that of the low-frequency mode, which shows that the spindle-tool structure is the most flexible part of the high-load robotic milling system. In other studies, the low-frequency modes caused by robot structure have higher dynamic flexibility. The spindle-tool structure is more sensitive to vibration, which may result in high-frequency chatter being first excited around the spindle-tool structure mode. This may be different from other research on mode coupling chatter in robotic milling.

3. Milling experiment

In the milling experiment, the initial posture of the robot and tool are consistent with the above dynamic characteristic test. The milling mode is selected as up milling, the workpiece is selected as 5A06 aluminum alloy, and the radial cutting depth a_e is selected as 2mm.

Without loss of generality, milling experiments are carried out when the feed direction angle γ is 0° and 90° respectively (the angle between the feed direction and the x-axis direction of the dynamic characteristic test). INV9822 acceleration sensor is used to collect acceleration signals during milling to determine whether chatter occurs. The experimental process is shown in Fig. 4.

The existing studies on mode coupling chatter in robot milling show that mode coupling chatter mainly occurs in low speed milling, while both mode coupling chatter and regenerative chatter may occur in high speed milling. In order to further explore the dominant chatter mechanism in high-load robot milling process, the spindle speed is divided into low speed (400–1000 rpm) and high speed (1000–8000 rpm) regions. Milling experiments with varying axial cutting depth are carried out at different speeds to determine the chatter stability boundary, as shown in Fig. 5. The specific process parameters during the milling experiments are shown in Table 1.

4. Experimental results and discussion

4.1. Analysis of milling experiment results at high speed region

When the feed direction angle γ is 0° and 90° , the milling experimental results under different speed are shown in the Fig. 6. ×

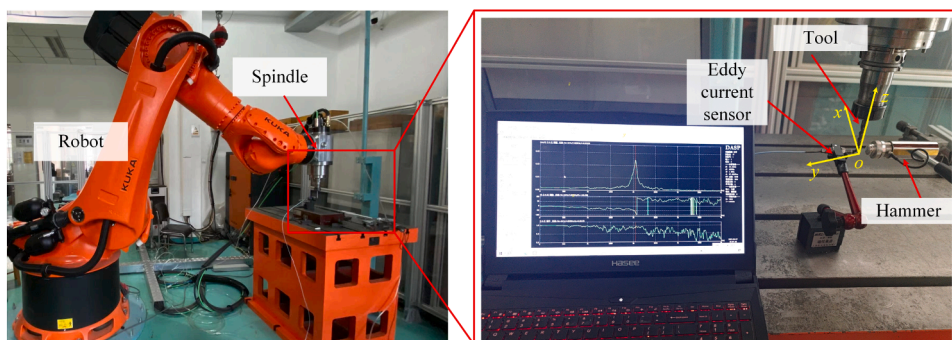


Fig. 1. The dynamic characteristic testing process of the robot milling system.

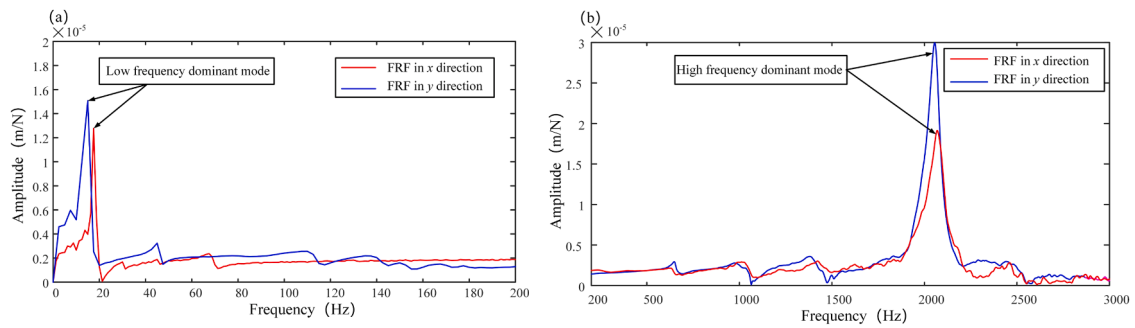


Fig. 2. The FRFs at the tool tip of the robot milling system (a) Low frequency dominant mode (b) High frequency dominant mode.

indicates that chatter occurs during milling with these parameters, and ● indicates that no chatter occurs with this parameters. The judgment of chatter is realized through the spectrum analysis of acceleration signal. Specifically, take the three chatter points A, B and C in Fig. 6 as an example, and their acceleration spectrum are shown in Fig. 7. Point A is the acceleration signal at the speed of 3000rpm. In its spectrum, the chatter frequencies (1895Hz, 2045Hz, 2345Hz) are observed, which are near the spindle-tool structural mode and different from spindle rotation frequency (50 Hz), tooth passing frequencies (150 Hz) and their harmonics (300 Hz). Therefore, the processing at point A is judged as chatter. Point B is the acceleration signal at the speed of 6000 rpm. It can be seen that high frequency components (2045.6Hz, 2345.6Hz) near the spindle-tool structure mode can be observed which are different from the spindle rotation frequency, tooth passing frequencies and their harmonics. Therefore, the processing at point B is judged as chatter. Point C is the acceleration signal at the speed of 6600 rpm. The obvious chatter frequency (1976.2 Hz, 2237.5 Hz, and 2567.5Hz) can also be observed in the spectrum. Point D is the acceleration signal at the speed of 3000 rpm, its acceleration spectrum contains only spindle rotation frequency, tooth passing frequencies and their harmonics. Therefore, the processing at point D is judged as steady. Points E (4800 rpm) and F (6600 rpm) are judged as chatter according to the above method.

By analyzing the acceleration spectrum at different milling speeds, it can be found that there are only spindle rotation frequency, tooth passing frequencies and their harmonics in the low frequency region. The chatter frequency is concentrated in the high frequency region which is close to the spindle-tool structural mode. However, in the low frequency region near the robot body structure mode, there is no chatter frequency which is different from the spindle rotation frequency, tooth passing frequencies and their harmonics. This is different from the conclusions obtained in Ref. [16] and Ref. [19]. In Ref. [16] and Ref. [19], a robot with a load of 205kg was used, and significant low-frequency chatter was observed during milling in the high-speed region. This may be due to the differences in the structural characteristics of the robot body. When the high-load robot is used for milling, the spindle-tool structure is more flexible than the body structure, and the spindle-tool structure mode is first excited to produce chatter during milling. According to the results of the previous research [7], the high-frequency chatter dominated by the spindle-tool mode is regenerative chatter. This shows that the milling chatter of the high-load robot in the high speed region is mainly regenerated chatter dominated by the spindle-tool structure mode.

4.2. Analysis of milling experiment results at low speed region

Similarly, the feed direction angle γ is set to 0° and 90° , and the robot milling experiments under different speeds are carried out in the low speed region. The experiment results are shown in Fig. 8. The acceleration signal is also used to determine whether the machining chatter occurs during milling process. Take the acceleration signal of points A, B, C and D in the figure as an example, and their spectrum is shown in the Fig. 9. Point A is the acceleration signal at the speed of 420 rpm. In its spectrum, 21Hz and 42Hz are the tool tooth passing frequencies and its harmonics, respectively. In addition, high amplitude frequency components (13.6 Hz) that are not equal to both the tooth passing frequency and its harmonics can be observed. Therefore, point A is judged to have occurred machining chatter. Point B is the acceleration signal at the speed of 540 rpm. It can be seen that high amplitude frequency components (13.5 Hz and 40.5 Hz) near the robot body structure mode can be observed which are different from the spindle rotation frequency (9 Hz), tooth passing frequency (18 Hz) and their harmonic (45Hz). Therefore, the processing at point B is judged as chatter. Point C is the acceleration signal at the speed of 420 rpm. In its spectrum, the chatter frequencies (15.8 Hz, 36.8 Hz) are observed, which are different from spindle rotation frequency, tooth passing frequencies and their harmonics. Therefore, the processing at point C is judged as chatter. Point D is the acceleration signal at the speed of 600 rpm. The obvious chatter frequency (15 Hz and 44.5Hz) can also be observed in the spectrum.

Through the above experimental results, it can be seen that the milling chatter signal component at low speed is concentrated in the low frequency region, which is similar to the robot body structure mode. No chatter component is observed in the high frequency region. This is consistent with the results obtained in Refs. [16,31,32]. This low frequency phenomenon indicates that when the high-load robot is used for milling in the low speed region, the robot body mode is excited to produce low frequency chatter. This may be due to the fact that the lower spindle speed makes the cutting frequency unable to excite the spindle-tool high frequency structural mode, thus the robot body low frequency structural mode is excited. In the present study (robot with lower load), the observed low frequency chatter is defined as mode coupling chatter. However, for high-load robot, the low frequency chatter mechanism of milling in low speed region needs to be further discussed.

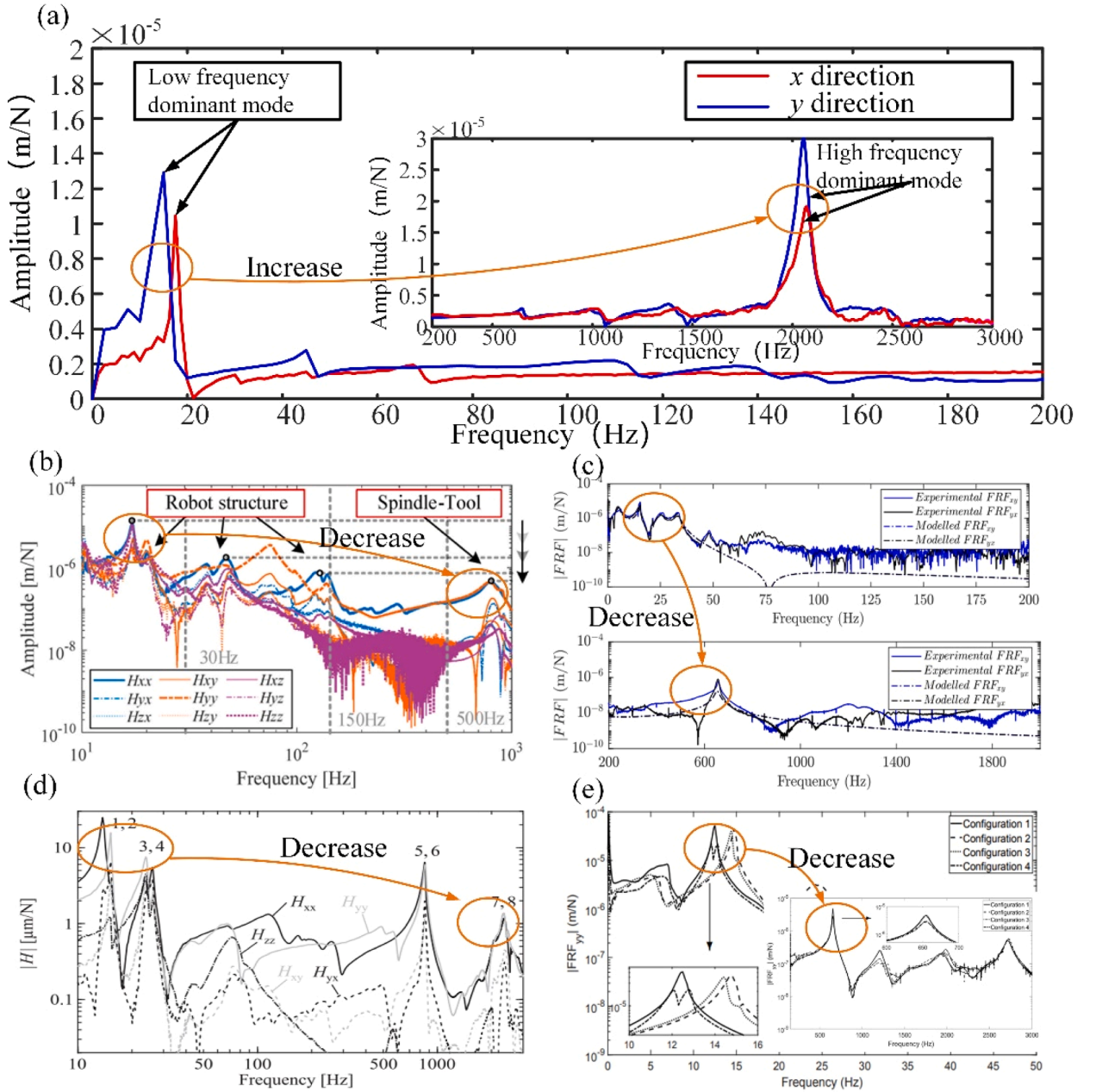


Fig. 3. The modal test results of robotic milling system. (a) The tool tip frequency response curve of the high-load robot milling system (600 kg) used in this paper. (b) Tool tip frequency response curve of robot milling system (205 kg), Fig. 3 in Ref. [18]. (c) Tool tip frequency response curve of robot milling system (205 kg), Fig. 5 in Ref. [35]. (d) Tool tip frequency response curve of robot milling system (205 kg), Fig. 3 in Ref. [13]. (e) Tool tip frequency response curve of robot milling system (205 kg), Fig. 5 in Ref. [23].

5. Analysis of low frequency chatter mechanism in high load robotic milling

In this section, a mode coupling chatter prediction model and a regenerative chatter prediction model are established based on the zeroth order approximation (ZOA) method. In order to ensure the generality of the research results, the eigenvalue method (EM) has also been applied to mode coupling chatter analysis, which is a commonly used analysis method for mode coupling chatter in robot milling in previous studies [16,17,28,31]. Based on the established model, the stability boundary of the mode coupling chatter is predicted and compared with the experimental results, so as to determine the low-frequency chatter mechanism of the high-load robot milling in the low-speed region.

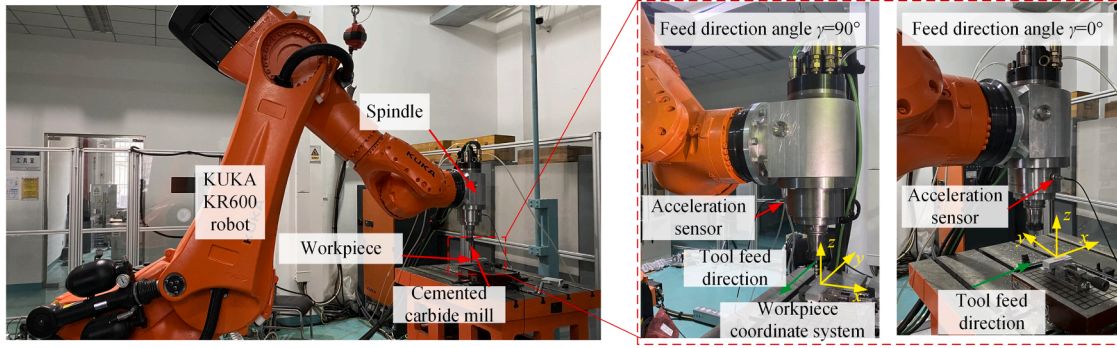


Fig. 4. The experimental process.

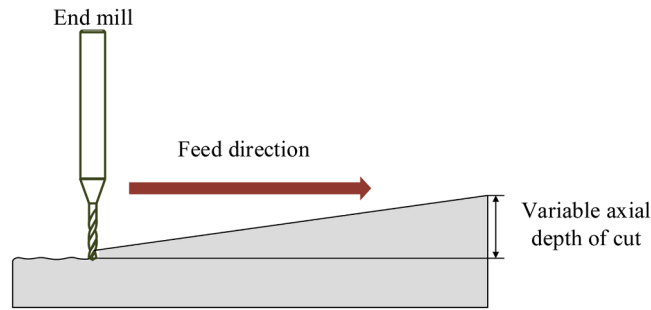


Fig. 5. Milling experiments with varying axial cutting depth.

Table 1

The process parameters during the milling experiments.

Feed direction Angle (°)	Spindle speed (rpm)	Feed speed (mm/min)	Radial cutting depth (mm)
0	420, 480, 540, 600, 660, 720, 800, 1800, 2400, 3000, 3600, 4200, 4800, 5400, 6000, 6600, 7200	600	2
90	420, 480, 540, 600, 660, 720, 800, 1800, 2400, 3000, 3600, 4200, 4800, 5400, 6000, 6600, 7200	600	2

5.1. Theory

(1) EM

In the predictive modeling of mode coupling chatter stability, the system dynamic is assumed to have two degrees of freedom, and the dynamic cutting thickness ignores the effect of regeneration. Firstly, the spatial relationship between each coordinate system in the milling process is defined, as shown in Fig. 10. Where $\{x_w-y_w\}$ is the workpiece coordinate system, and the direction of its x -axis is the same as the direction of x during the dynamic characteristic test. $\{x_c-y_c\}$ is the tool coordinate system, and the angle between the x_c -axis and the x_w -axis is set to γ . $\{x_k-y_k\}$ is the principal stiffness coordinate system of the robot, and the angle between x_k and the x_c -axis is set to α_0 . F is the cutting force vector in the milling process, and the angle between it and the workpiece coordinate system and the main stiffness coordinate system x -axis is set to β_0 and γ_0 , respectively. Δ is the vector of the dynamic displacement, and the angle between it and the x_w -axis is set to θ_0 .

Since damping always improves the stability of the system, the system is assumed to be undamped as in previous studies [16,28]. The two-degree-of-freedom milling dynamics model can be expressed as follow:

$$\begin{bmatrix} m_k & 0 \\ 0 & m_k \end{bmatrix} \begin{bmatrix} \ddot{x}_k \\ \ddot{y}_k \end{bmatrix} + \begin{bmatrix} k_x & 0 \\ 0 & k_y \end{bmatrix} \begin{bmatrix} x_k \\ y_k \end{bmatrix} = \begin{bmatrix} k_p \cos \gamma_0 (A \cos \alpha_0 + B \sin \alpha_0) & k_p \cos \gamma_0 (-A \sin \alpha_0 + B \cos \alpha_0) \\ k_p \sin \gamma_0 (A \cos \alpha_0 + B \sin \alpha_0) & k_p \sin \gamma_0 (-A \sin \alpha_0 + B \cos \alpha_0) \end{bmatrix} \begin{bmatrix} x_k \\ y_k \end{bmatrix} \quad (1)$$

where

$$A = \cos \theta_0 \cos \gamma - \sin \theta_0 \sin \gamma \quad (2)$$

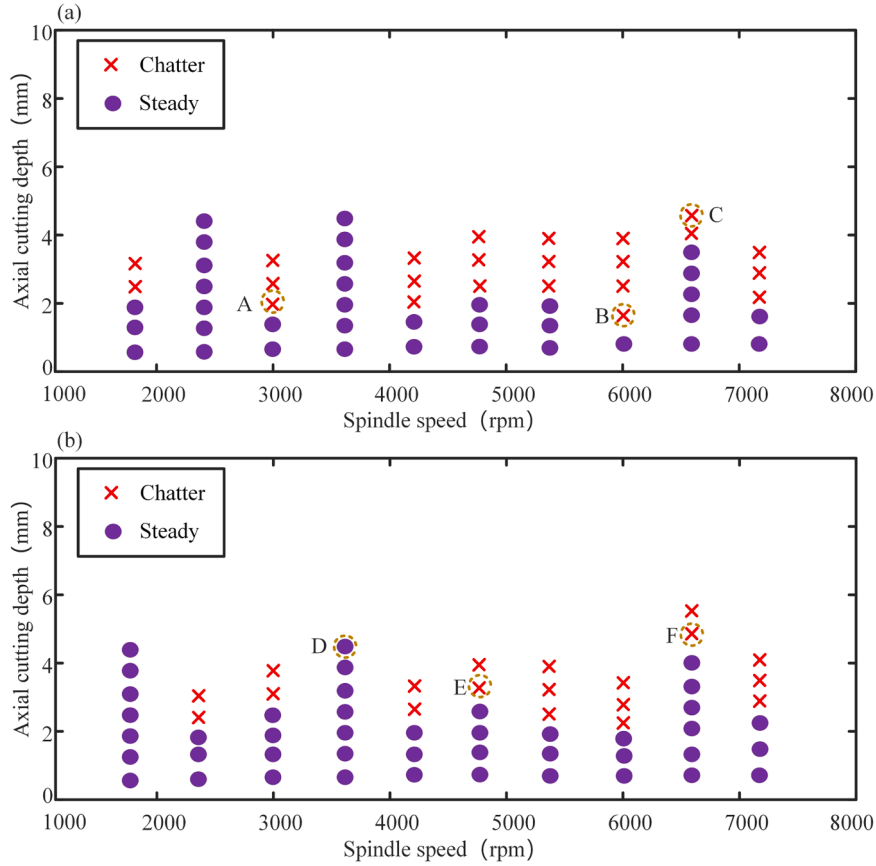


Fig. 6. The milling experimental results under different speed. (a) The feed direction angle γ is 0° (b) The feed direction angle γ is 90°

$$B = \cos\theta_0 \sin\gamma + \sin\theta_0 \cos\gamma \quad (3)$$

Where, m_k represents the elements after the mass matrix of the robot body is decoupled, k_x and k_y represent the elements of the matrix after the stiffness matrix of the robot is decoupled, and the specific calculation process can be found in the Ref. [36]. k_p stands for cutting stiffness, which can be expressed by the differential of the cutting force to the displacement [31], as shown in Eq. (4):

$$k_p = \frac{dF}{d\Delta} = \frac{d\sqrt{\bar{F}_{xw}^2 + \bar{F}_{yw}^2}}{dx_w \cos\theta_0 + dy_w \sin\theta_0} \quad (4)$$

Where, A and B are the components of the average cutting force in the x and y directions of the workpiece coordinate system. The cutting force can be calculated by the micro-element method, and the specific calculation process can be obtained from Refs. [37–39]. Then the Eq. (1) can be transformed into the following form:

$$\begin{bmatrix} \ddot{x}_k \\ \ddot{y}_k \end{bmatrix} = \begin{bmatrix} \frac{k_x - k_p \cos\gamma_0 (A \cos\alpha_0 + B \sin\alpha_0)}{m_k} & \frac{k_p \cos\gamma_0 (-A \sin\alpha_0 + B \cos\alpha_0)}{m_k} \\ \frac{k_p \sin\gamma_0 (A \cos\alpha_0 + B \sin\alpha_0)}{m_k} & \frac{k_y - k_p \sin\gamma_0 (-A \sin\alpha_0 + B \cos\alpha_0)}{m_k} \end{bmatrix} \begin{bmatrix} x_k \\ y_k \end{bmatrix} \quad (5)$$

The above formula is integrated as follows:

$$k'_x = k_x - k_p \cos\gamma_0 (A \cos\alpha_0 + B \sin\alpha_0) \quad (6)$$

$$k'_y = k_y - k_p \sin\gamma_0 (-A \sin\alpha_0 + B \cos\alpha_0) \quad (7)$$

Therefore, the characteristic equation of Eq. (5) can be expressed as follow:

$$\lambda^2 + \frac{k'_x + k'_y}{m_k} \lambda + \frac{k'_x k'_y + \frac{1}{4} k_p^2 \sin(2\gamma_0) [(A^2 - B^2) \sin(2\alpha_0) - 2AB \cos(2\alpha_0)]}{m_k^2} = 0 \quad (8)$$

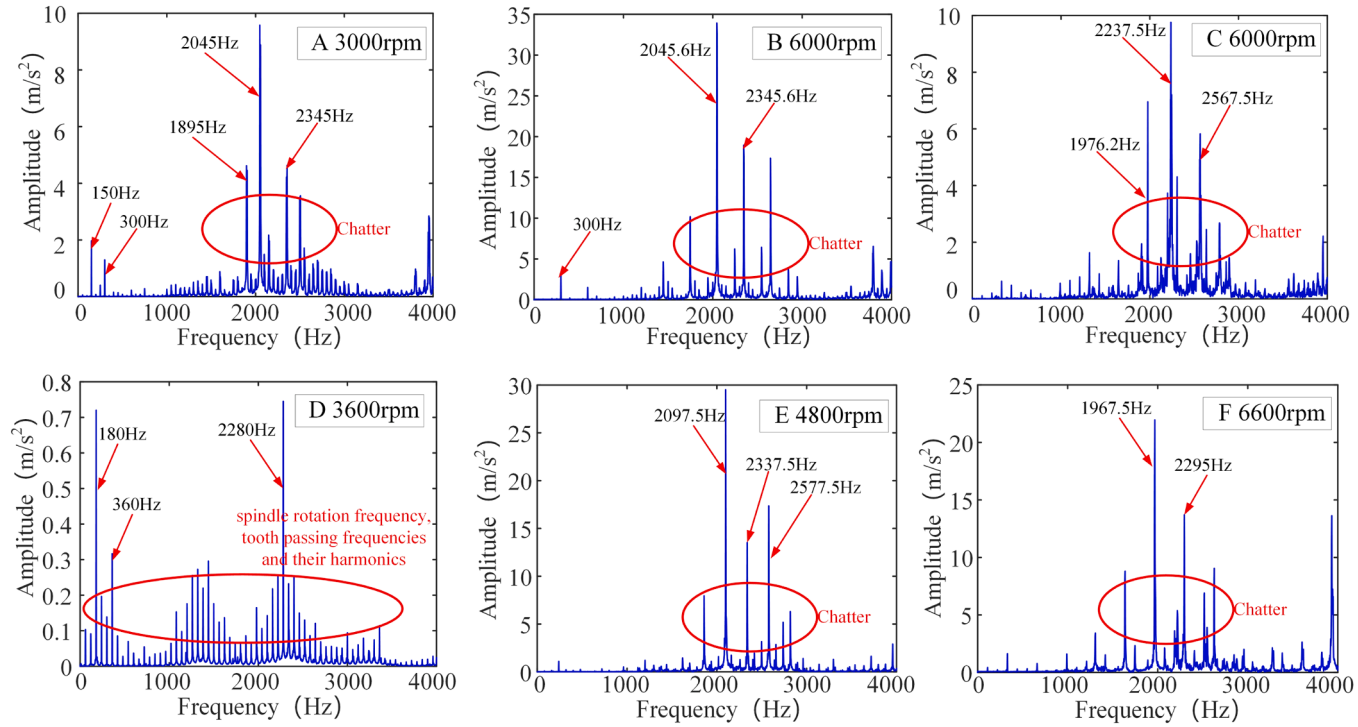


Fig. 7. Spectrum analysis of measuring point acceleration.

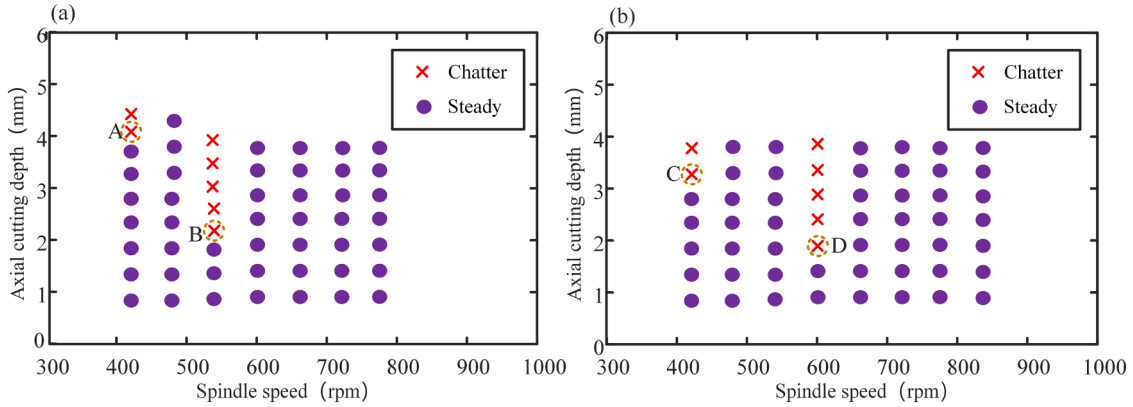


Fig. 8. The milling experimental results under different speed (a) The feed direction angle γ is 0° (b) The feed direction angle γ is 90°

where

$$\lambda = \frac{-(k'_x + k'_y) \pm \sqrt{(k'_x - k'_y)^2 - k_p^2 \sin(2\gamma_0) [(A^2 - B^2) \sin(2\alpha_0) - 2AB \cos(2\alpha_0)]}}{2m_k} \quad (9)$$

According to the identification conditions for mode coupling chatter proposed in Refs. [21], the system is in an unstable state when the eigenvalue λ is plural. That is, when Eq. (10) is true, the robot milling process will occur mode coupling chatter.

$$(k'_x - k'_y)^2 - k_p^2 \sin(2\gamma_0) [(A^2 - B^2) \sin(2\alpha_0) - 2AB \cos(2\alpha_0)] < 0 \quad (10)$$

(2) ZOA

When the mode coupling chatter stability is predicted by ZOA, it is still assumed that the dynamic cutting thickness is only related to the vibration generated by the current tool teeth, and the surface left by the previous tool teeth is ignored. The milling process is shown in the Fig. 11. The cutting force term can be expressed in the following form:

$$\mathbf{F} = \begin{bmatrix} F_{xw} \\ F_{yw} \end{bmatrix} = \frac{1}{2} a_p K_{tc} \mathbf{A}(t) \Delta(t) \quad (11)$$

in which, $\Delta(t)$ is

$$\Delta(t) = \begin{bmatrix} x_w(t) \\ y_w(t) \end{bmatrix} \quad (12)$$

$\mathbf{A}(t)$ is the time-varying dynamic cutting force coefficient matrix in the milling process, and its expression is

$$\mathbf{A}(t) = \begin{bmatrix} \sum_{j=1}^N -g(\varphi_j) [\sin 2\varphi_j + K_r (1 - \cos 2\varphi_j)] & \sum_{j=1}^N -g(\varphi_j) [1 + \cos 2\varphi_j + K_r \sin 2\varphi_j] \\ \sum_{j=1}^N g(\varphi_j) [1 - \cos 2\varphi_j - K_r \sin 2\varphi_j] & \sum_{j=1}^N g(\varphi_j) [\sin 2\varphi_j - K_r (1 + \cos 2\varphi_j)] \end{bmatrix} \quad (13)$$

Where, φ_{jm} represents the instantaneous engagement angle between the tool and the workpiece, and K_r is the ratio of the radial cutting force coefficient K_{rc} (270.93 N/mm²) to the tangential cutting force coefficient K_{tc} (855.00 N/mm²).

By further Fourier expansion of $\mathbf{A}(t)$, Eq. (11) can be transformed into the following form:

$$\mathbf{F}(t) = \frac{1}{2} a_p K_{tc} \mathbf{A}_0 \Delta(t) \quad (14)$$

where

$$\mathbf{A}_0 = \frac{N}{2\pi} \begin{bmatrix} a_{xx} & a_{xy} \\ a_{yx} & a_{yy} \end{bmatrix} = \frac{N}{2\pi} \begin{bmatrix} \frac{1}{2} [\cos 2\varphi_{jm} - 2K_r \varphi_{jm} + K_r \sin 2\varphi_{jm}]_{\varphi_{en}}^{\varphi_{ex}} & \frac{1}{2} [-\sin 2\varphi_{jm} - 2\varphi_{jm} + K_r \cos 2\varphi_{jm}]_{\varphi_{en}}^{\varphi_{ex}} \\ \frac{1}{2} [-\sin 2\varphi_{jm} + 2\varphi_{jm} + K_r \cos 2\varphi_{jm}]_{\varphi_{en}}^{\varphi_{ex}} & \frac{1}{2} [-\cos 2\varphi_{jm} - 2K_r \varphi_{jm} - K_r \sin 2\varphi_{jm}]_{\varphi_{en}}^{\varphi_{ex}} \end{bmatrix} \quad (15)$$

φ_{en} and φ_{ex} are the cutting entry and exit boundary angles respectively.

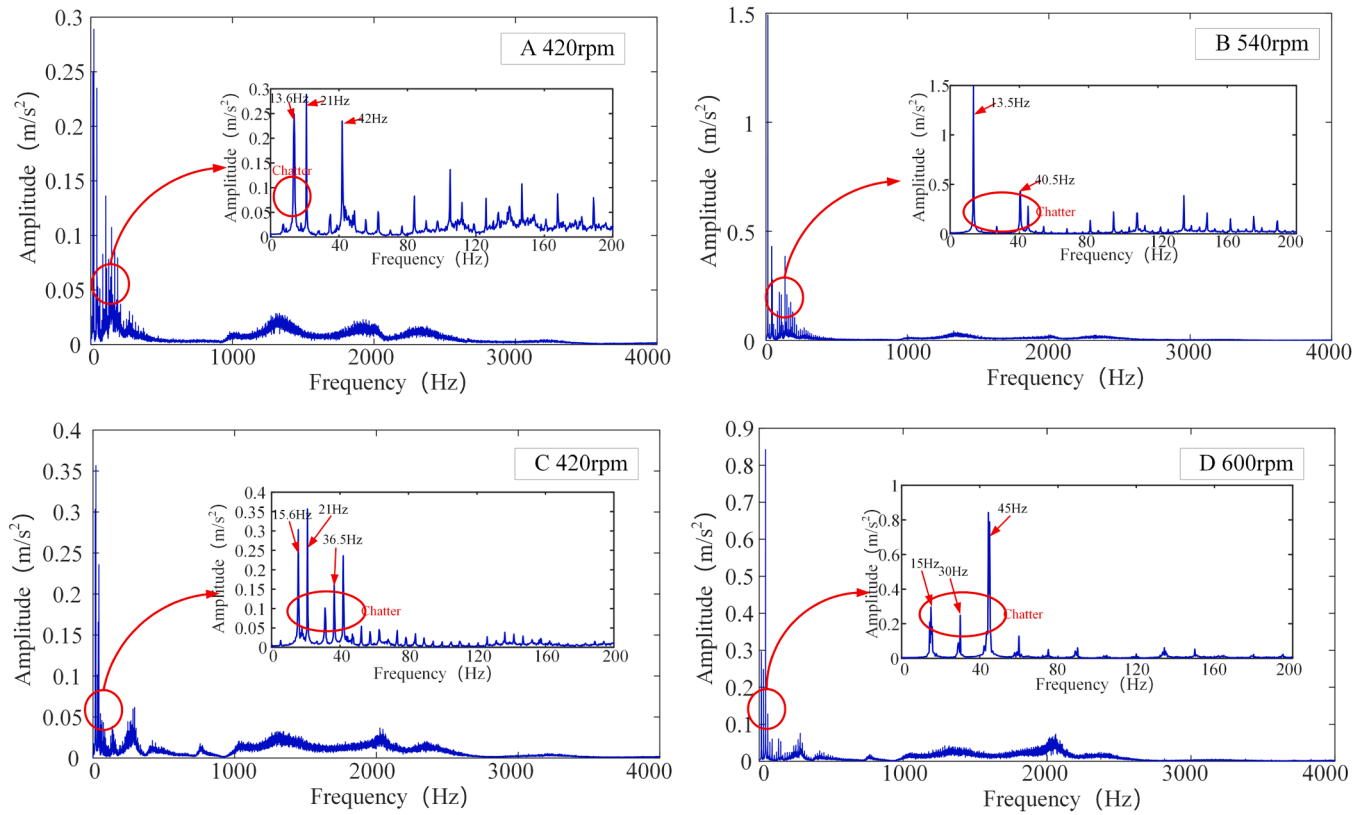


Fig. 9. Spectrum analysis of measuring point acceleration.

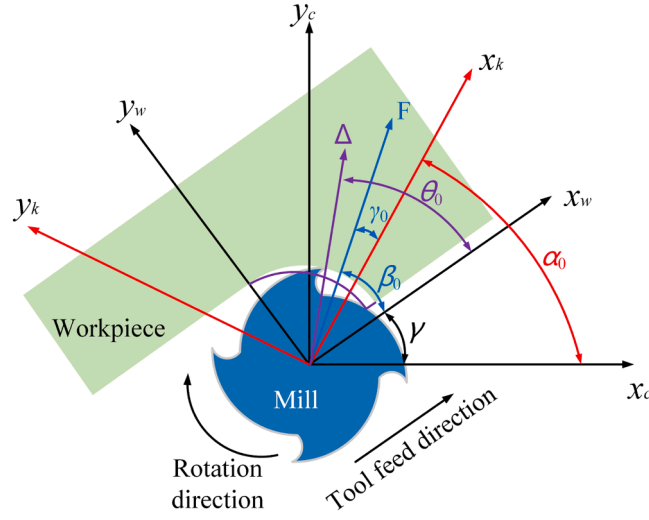


Fig. 10. The spatial relationship between each coordinate system in the milling process.

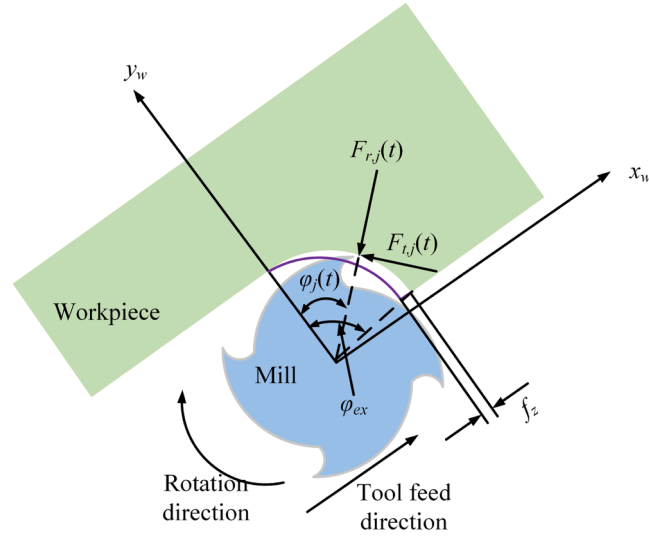


Fig. 11. The milling process.

The vibration displacement $\Delta(t)$ is expressed in the frequency domain by a harmonic function, then the vibration displacement at the chatter frequency ω_c can be expressed as follow:

$$\Delta(i\omega_c) = \mathbf{FRF}(i\omega_c)\mathbf{F}e^{i\omega_c t} \quad (16)$$

where $\mathbf{FRF}(i\omega)$ represents the frequency response function of the robotic milling system:

$$\mathbf{FRF}(i\omega) = \begin{bmatrix} \mathbf{FRF}_{xx}(i\omega) & \mathbf{FRF}_{xy}(i\omega) \\ \mathbf{FRF}_{yx}(i\omega) & \mathbf{FRF}_{yy}(i\omega) \end{bmatrix} \quad (17)$$

Then Eq. (14) can be further transformed into the following form:

$$\mathbf{F}e^{i\omega_c t} = \frac{1}{2}a_p K_{tc} \mathbf{A}_0 \mathbf{FRF}(i\omega_c) e^{i\omega_c t} \mathbf{F} \quad (18)$$

The characteristic equation can be expressed as the following form:

$$\det[\mathbf{I} + \lambda \mathbf{FRF}_0(i\omega_c)] = 0 \quad (19)$$

where

$$\mathbf{FRF}_0(i\omega_c) = \begin{bmatrix} a_{xx}FRF_{xx}(i\omega_c) + a_{xy}FRF_{yx}(i\omega_c) & a_{xx}FRF_{xy}(i\omega_c) + a_{xy}FRF_{yy}(i\omega_c) \\ a_{yx}FRF_{xx}(i\omega_c) + a_{yy}FRF_{yx}(i\omega_c) & a_{yx}FRF_{xy}(i\omega_c) + a_{yy}FRF_{yy}(i\omega_c) \end{bmatrix} \quad (20)$$

The eigenvalue λ can be solved in the following form:

$$\lambda = -\frac{a_1 \pm \sqrt{a_1^2 - 4a_0}}{2a_0} \quad (21)$$

where

$$a_0 = (a_{xx}a_{yy} - a_{xy}a_{yx})(FRF_{xx}(i\omega_c)FRF_{yy}(i\omega_c) - FRF_{xy}(i\omega_c)FRF_{yx}(i\omega_c)) \quad (22)$$

$$a_1 = a_{xx}FRF_{xx}(i\omega_c) + a_{xy}FRF_{yx}(i\omega_c) + a_{yx}FRF_{xy}(i\omega_c) + a_{yy}FRF_{yy}(i\omega_c) \quad (23)$$

Because the frequency response function is plural, the eigenvalue has real and imaginary parts, which can be expressed as:

$$\lambda = \lambda_R + i\lambda_I \quad (24)$$

By combining Eqs. (18) - (24), the limit cutting depth at the chatter frequency ω_c can be calculated:

$$a_{plim} = -\frac{4\pi}{NK_{tc}}(\lambda_R + i\lambda_I) \quad (25)$$

In order to make a_{plim} positive real number. The eigenvalue must have an imaginary part of 0 and a negative real part. Then Eq. (25) can be converted to the following form:

$$a_{plim} = -\frac{4\pi}{NK_{tc}}\lambda_R \quad (26)$$

The stability boundary of mode coupling chatter can be calculated according to Eq. (26).

5.2. Analysis of chatter stability prediction results

In the low speed region, when the feed direction angle γ is 0° , the comparison between the experimental results and the prediction results is shown in Fig. 12. In the figure, the regions above different curves represent the chatter occurrence regions predicted by different methods, and the regions below the curves represent the predicted stable processing regions. According to the criterion Eq. (10), the prediction results based on EM show that the mode coupling chatter will not occur when the feed direction angle is 0 . Therefore, the chatter stability boundary predicted by EM is not shown in the figure. It can be seen from the figure that the chatter stability boundary predicted by ZOA has the same critical cutting depth at different speeds. This is because in the milling dynamics model, $\Delta(t)$ is the dynamic cutting thickness generated by the current tool tooth vibration in the milling process, which is only related to the current tool tooth vibration and has nothing to do with the tool tooth passing period T . Therefore, the change of the chatter stability boundary does not depend on the spindle speed, and it appears as a straight line. In addition, the regenerative chatter stability boundary based on ZOA is also predicted, as shown by the pink curve in the figure.

The results of comparison between the robot milling experiment and the stability boundary prediction show that the stability boundary of the mode coupling chatter predicted by the two methods is obviously inconsistent with the experimental results. The chatter stability boundary of mode coupling chatter predicted by EM shows that when the feed direction angle γ is 0° , mode coupling chatter will not occur in milling process. However, the milling experiment results show that the robot milling process will have obvious chatter phenomenon under different speeds. The predicted mode coupling chatter stability boundary by ZOA has a rather low limit axial cutting depth, but the experimental chatter stability boundary is obviously much higher than the predicted result. In addition, the predicted mode coupling chatter stability boundary by ZOA does not change with the change of speed, and the experimental results show that the chatter is strongly dependent on the change of spindle speed, and there are different critical cutting depths at different speeds.

The results of milling experiment and chatter stability boundary prediction are compared when the feed direction angle γ is 90° . It can be seen from Fig. 13 that the chatter stability boundary predicted by EM gradually increases with the increase of the spindle speed, which is almost linearly correlated with the spindle speed. However, in the experimental results, the occurrence of chatter is related to the spindle speed and presents periodic characteristics. Therefore, when the feed direction angle γ is 90° , the mode coupling chatter theory based on EM still cannot explain the low-frequency chatter behavior during milling. The characteristics of the chatter stability boundary predicted by ZOA are consistent with those when the feed direction angle γ is 0° , which is also inconsistent with the experimental results.

In conclusion, the mode coupling chatter theory based on EM and ZOA cannot explain the low-frequency chatter phenomenon in the experiment. By comparing the regenerative chatter stability boundary with the experimental results, it can be found that although the predicted stability boundary based on the regenerative chatter theory does not match the experimental results to some extent, the stability boundary changes periodically with the change of spindle speed. Therefore, the regenerative chatter theory can explain the dependence of stability boundary on spindle speed. The discrepancy between the theoretical prediction and the experimental results may be caused by the failure to consider the complex interaction between the robot and the process in the dynamics model. However,

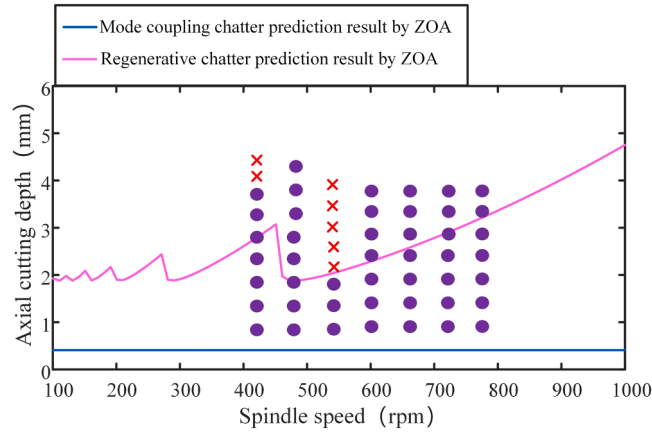


Fig. 12. The comparison between the experimental results and the prediction results.

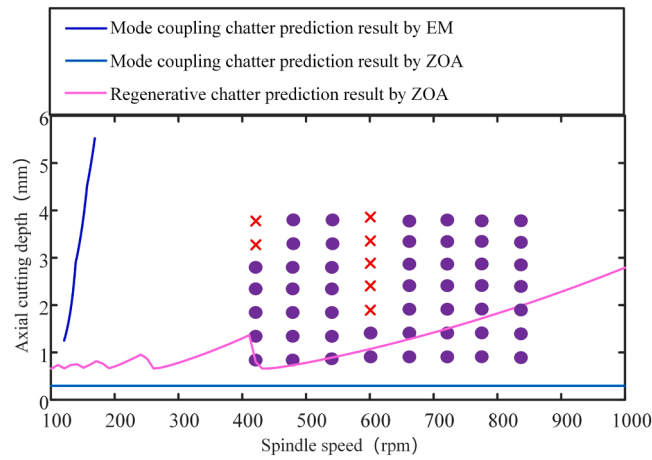


Fig. 13. The comparison between the experimental results and the prediction results.

these differences are reflected in the level of stability boundary at different speeds, and it does not change the trend that the stability boundary changes with the spindle speed. Therefore, the milling chatter mechanism of the high-load robot in the low speed region still belongs to regenerative chatter, which is dominated by the robot body structure mode.

6. Conclusion

The dynamic characteristics of high-load robots are quite different from those of low-load robots, mainly in that the dynamic flexibility of the high-frequency mode is significantly higher than that of the low-frequency mode, which may affect the milling chatter behavior. In order to achieve effective control of chatter, the dominant chatter mechanism of the high-load robot is investigated in this study.

Robot milling experiments are carried out at different speed regions, and the distribution characteristics of chatter with process parameters are analyzed. Based on eigenvalue method (EM) and zeroth order approximation (ZOA), the stability prediction models of mode coupling chatter are established, and the predicted stability boundaries are compared with the experimental results. The results show that the chatter in the high speed region is around the high frequency mode of spindle-tool, and no low frequency chatter occurs. The low-frequency chatter around the robot body mode in the low-speed region is found, but the mode coupling chatter theory could not explain the periodic change of low-frequency chatter with the spindle speed. By comparing the regenerative chatter stability boundary with the experimental results, it can be found that although the predicted stability boundary based on the regenerative chatter theory does not match the experimental results to some extent, the stability boundary changes periodically with the change of spindle speed. Therefore, the regenerative chatter theory can explain the dependence of stability boundary on spindle speed. This indicates that the milling chatter dominant mechanism of high load robot is regenerative chatter.

CRediT authorship contribution statement

Yuchao Du: Writing – original draft, Methodology, Investigation, Formal analysis, Data curation, Conceptualization. **Zhiqiang Liang:** Writing – review & editing, Supervision, Funding acquisition. **Zirui Gao:** Writing – review & editing, Validation, Software, Investigation. **Sichen Chen:** Visualization, Methodology, Investigation. **Yi Yue:** Writing – review & editing, Investigation. **jiabo Zhang:** Writing – review & editing, Investigation. **Hanliang Liu:** Writing – review & editing. **Haoran Zheng:** Validation. **Baolong Liu:** Writing – review & editing, Visualization. **Tianyang Qiu:** Writing – review & editing, Supervision. **Zhibing Liu:** Supervision.

Declaration of competing interest

The authors declare that they have no known competing financial interests or personal relationships that could have appeared to influence the work reported in this paper.

Acknowledgments

The research was supported by the National Natural Science Foundation of China (No. 52375400), the China Postdoctoral Science Foundation (2024M764124), Inversion and Application Project of Outcome (Nos. CA2EFD46 and FCB6032B) and Basic Research Program (No. DEDPCL).

Data availability

Data will be made available on request.

References

- [1] Z. Liao, J. Li, H. Xie, Q. Wang, X. Zhou, Region-based tool path generation for robot milling of freeform surfaces with stiffness optimization, *Robot. Comput. Integr. Manuf.* 64 (2020) 101953.
- [2] D. Zhu, X. Feng, X. Xu, Z. Yang, W. Li, S. Yan, H. Ding, Robot grinding of complex components: a step towards efficient and intelligent machining – challenges, solutions, and applications, *Robot. Comput. Integr. Manuf.* 65 (2020) 101908.
- [3] Z. Zhu, X. Tang, C. Chen, F. Peng, R. Yan, L. Zhou, Z. Li, J. Wu, High precision and efficiency robot milling of complex parts: challenges, approaches and trends, *Chin. J. Aeronaut.* 35 (2022) 22–46.
- [4] H. Huynh, H. Assadi, V. Dambly, E. Rivière-Lorphèvre, O. Verlinden, Direct method for updating flexible multibody systems applied to a milling robot, *Robot. Comput. Integr. Manuf.* 68 (2021) 102049.
- [5] Y. Guo, H. Dong, Y. Ke, Stiffness-oriented posture optimization in robotic machining applications, *Robot. Comput. Integr. Manuf.* 35 (2015) 69–76.
- [6] I. Iglesias, M. Sebastián, J.E. Ares, Overview of the state of robotic machining: current situation and future potential, *Procedia Eng.* 132 (2015) 911–917.
- [7] L. Yuan, Z. Pan, D. Ding, S. Sun, W. Li, A review on chatter in robot machining process regarding both regenerative and mode coupling mechanism, *IEEE-Asme T Mech.* 23 (2018) 2240–2251.
- [8] M. Tran, M. Liu, M. Elsis, Effective multi-sensor data fusion for chatter detection in milling process, *ISA Trans.* 125 (2022) 514–527.
- [9] J. Munoa, X. Beudaert, Z. Dombvari, Y. Altintas, E. Budak, C. Brecher, G. Stepan, Chatter suppression techniques in metal cutting, *CIRP Ann. - Manuf Technol.* 65 (2016) 785–808.
- [10] D. Wang, M. Löser, S. Ihlenfeldt, X.B. Wang, Z.B. Liu, Milling stability analysis with considering process damping and mode shapes of in-process thin-walled workpiece, *Int. J. Mech. Sci.* 159 (2019) 382–397.
- [11] Y. Altintas, *Manufacturing Automation: Metal Cutting Mechanics, Machine Tool Vibrations, and CNC Design*, Cambridge University Press, 2012.
- [12] G. Quintana, J. Ciurana, Chatter in machining processes: a review, *Int. J. Mach. Tools. Manuf.* (51) (2011) 363–376.
- [13] M. Cordes, W. Hintze, Y. Altintas, Chatter stability in robot milling, *Robot. Comput. Integr. Manuf.* 55 (2019) 11–18.
- [14] J. Tlustý, F. Ismail, Basic non-linearity in machining chatter, *CIRP Ann. Manuf. Technol.* 30 (1) (1981) 299–304.
- [15] B. Stone, *Chatter and Machine Tools*, Springer, 2014.
- [16] Z. Pan, H. Zhang, Z. Zhu, J. Wang, Chatter analysis of robot machining process, *J Mater Process Tech* 173 (2006) 301–309.
- [17] R. Wang, F. Li, J. Niu, Y. Sun, Prediction of pose-dependent modal properties and stability limits in robotic ball-end milling, *Robot. Comput. Integr. Manuf.* 75 (2022) 102307.
- [18] S. Xin, F. Peng, X. Tang, R. Yan, Z. Li, Research on the influence of robot structural mode on regenerative chatter in milling and analysis of stability boundary improvement domain, *Int. J. Mach. Tools. Manuf.* 179 (2022) 103918.
- [19] S. Xin, X. Tang, F.J. Wu, R. Yan, W. Yang, Investigation of the low-frequency chatter in robotic milling, *Int. J. Mach. Tools. Manuf.* 190 (2023) 104048.
- [20] Y. Mohammadi, K. Ahmadi, Effect of axial vibrations on regenerative chatter in robotic milling, *Procedia CIRP.* 82 (2019) 503–508.
- [21] Y. Mohammadi, K. Ahmadi, Chatter in milling with robots with structural nonlinearity, *Mech. Syst. Signal Pr.* 167 (2022) 108523.
- [22] Y. Du, Z. Liang, S. Chen, et al., Dynamic modeling and stability prediction of robot milling considering the influence of force-induced deformation on regenerative effect and process damping, *Metals* (Basel) 13 (2023) 974.
- [23] H. Celikog, D.S. Neil, E. Ozturk, Chatter suppression in robotic milling by control of configuration dependent dynamics, *Proc. CIRP.* 82 (2019) 521–526.
- [24] S. Mousavi, V. Gagnol, B.C. Bouzgarrou, P. Ray, Control of a multi degrees functional redundancies robotic cell for optimization of the machining stability, *Proc. CIRP.* 58 (2017) 269–274.
- [25] S. Mousavi, V. Gagnol, B.C. Bouzgarrou, P. Ray, Guo, Stability optimization in robotic milling through the control of functional redundancies, *Robot. Comput. Integr. Manuf.* 50 (2018) 181–192.
- [26] F. Chen, H. Zhao, Design of eddy current dampers for vibration suppression in robotic milling, *Adv. Mech. Eng.* 10 (11) (2018) 1–15.
- [27] L. Sun, K. Zheng, W. Liao, et al., Investigation on chatter stability of robotic rotary ultrasonic milling, *Robot. Comput. Integr. Manuf.* 63 (2020) 101911.
- [28] F. He, Y. Liu, K. Liu, A chatter-free path optimization algorithm based on stiffness orientation method for robotic milling, *Int. J. Adv. Manuf. Technol.* 101 (2019) 2739–2750.
- [29] O. Gienke, Z. Pan, L. Yuan, T. Lepper, S. Duin, A full-discretization method for prediction of milling stability, *Int. J. Adv. Manuf. Technol.* 104 (2019) 2103–2116.
- [30] Z. Pan, H. Zhang, Analysis and Suppression of Chatter in Robotic Machining Process, in: *International Conference on Control, Automation and Systems*, COEX, Seoul, Korea, 2007. Oct. 17–20.
- [31] L. Cen, S. Melkote, CCT-based mode coupling chatter avoidance in robotic milling, *J. Manuf. Process.* 29 (2017) 50–61.
- [32] L. Cen, S. Melkote, J. Castle, H. Appelman, A method for mode coupling chatter detection and suppression, *J. Manuf. Sci. E-T Asme.* 140 (2018), 081015-1-9.

- [33] L. Yuan, S. Sun, Z. Pan, et al., Mode coupling chatter suppression for robotic machining using semi-active magnetorheological elastomers absorber, *Mech. Syst. Signal Pr.* 117 (2019) 221–237.
- [34] C. Chen, F. Peng, R. Yan, X. Tang, Y. Li, Z. Fan, Rapid prediction of posture-dependent FRF of the tool tip in robotic milling, *Robot. Comput. Integr. Manuf.* 64 (2020) 101906.
- [35] H. Celikag, E. Ozturk, N.D. Sims, Can mode coupling chatter happen in milling? *Int. J. Mach. Tools. Manuf.* 165 (2021) 103738.
- [36] J. Yang, X. Zhang, Y. Wu, S. Ye, S. Yan, J. Lu, Posture Optimization based on Stiffness orientation method for industrial robot milling, *Chin. Mech. Eng.* 33 (2022) 1957–1964.
- [37] Y. Sun, S. Jiang, Predictive modeling of chatter stability considering force-induced deformation effect in milling thin-walled parts, *Int. J. Mach. Tools. Manuf.* 135 (2018) 38–52.
- [38] S. Jiang, Y. Sun, Stability analysis for a milling system considering multi-point-contact cross-axis mode coupling and cutter run-out effects, *Mech. Syst. Signal Pr.* 141 (2020) 106452.
- [39] Z. Li, O. Tuysuz, L. Zhu, Y. Altintas, Surface form error prediction in five-axis flank milling of thin-walled parts, *Int. J. Mach. Tools. Manuf.* 128 (2018) 21–32.